Optimization of band-limited DSP-aided 25 and 50 Gbps PON using 10G-class DML and APD

Optimization of band-limited DSP-aided 25 and 50 Gbps PON using 10G-class DML and APD

Pablo Torres-Ferrera, Haoyi Wang, Valter Ferrero, *Senior Member, IEEE*, Maurizio Valvo and Roberto Gaudino, *Senior Member, IEEE*

***Abstract*—The increasing demand for network capacity is driving the development of next-generation high-speed Passive Optical Networks (PON) supporting 25 and 50 Gbps. One solution to reduce transceiver cost is reusing the 10G-class optical transmitter (including Directly Modulated Lasers, DML, in O-band) and receiver components in combination with Digital Signal Processing (DSP) techniques to compensate for bandwidth limitations. In this paper, by means of both a set of laboratory experiments and a metropolitan field demonstrator, we discuss practical PON solutions at 25 and 50 Gbps per wavelength and per direction. In terms of modulation formats, we compare 2-level pulse amplitude modulation (PAM-2), 4-level PAM (PAM-4) and electrical duobinary (EDB) modulation formats, with feed-forward (FFE) and decision-feedback (DFE) adaptive equalizer at the receiver side. The novelty of our paper is manifold. First, we present an optimization in terms of optical receiver band requirements for the 50 Gbps transmission. We show, by means of experimental measurements and numerical simulations, the minimum required bandwidth for DML laser and APD receiver (with appropriate DSP techniques) to realize next generation 25 and 50 Gbps PON transceivers. Second, we discuss also the upstream point of view, with a specific focus on DSP, and in particular, we propose an experimental solution based on a burst mode receiver with memory-aided DSP technique, together with a novel DSP approach to overcome the typical AC coupling distortion due to the burst mode scenario. Finally, we show a coexistence experiment between XGS-PON and 25 Gbps PON on an installed metropolitan field trial.**

***Index Terms*— Passive Optical Networks, Filtering, Avalanche Photodiode, Adaptive Equalization, PAM, Duobinary modulation.**

I. Introduction

The ever increasing bandwidth demand at all network levels, including at the edges to the final user, is motivating the continuous increase of Passive Optical Networks (PON) towards higher bit rates. New PON standardization proposals are rapidly evolving and are today addressing the definition of 25 Gbps PON (25G-PON) and 50 Gbps PON (50G-PON) [1-3]. Among several research directions to develop the next generation of 25G- and 50G-PON physical layer, we can identify two main approaches. The first one, aimed to design low cost transceivers, is based on reusing the already existing optoelectronic components developed for 10 Gbps PON, solving the resulting strong bandwidth limitations by proper Digital Signal Processing (DSP) techniques, such as adaptive equalization and the use of more efficient modulation formats [4-17]. The other alternative places greater weight on the development of broader bandwidth hardware thus reducing or avoiding the DSP complexity of the transceivers [4, 18, 19]. In this paper, we focus on the former approach: band-limited DSP-aided PON systems. In recent years, several solutions based on machine learning or other high-complex DSP techniques (such as Volterra-based equalizers) were proposed in order to compensate the strong bandwidth limitations, the impact of chirp and chromatic dispersion and nonlinearities in PON systems [10-17]. However, these solutions are critical to be implemented in the mid-term and in the PON area due to their high complexity and current hardware and software limitations, particularly because in downstream transmission these highly complex DSP need to be placed in Optical Network Units (ONU) at the user side, which is the most cost-constrained element. In our present paper, we thus decide to focus on more realistic DSP implementations and, moreover, we studied both upstream and downstream transmission. In particular, we propose PON systems using existing commercial 10G-class optoelectronics, such as Directly Modulated Lasers (DML) and avalanche photodiodes (APD), operating in O-band to avoid optical or digital dispersion compensation. Moreover, just as a comparison with APD-based receivers, we also give some preliminary results on semiconductor optical amplifier (SOA)+PIN-based receivers. The capability of "native" 10G-class optoelectronics is "stretched" to 25 and 50 Gbps in our paper using the following DSP-techniques:

- Adaptive equalization at the receiver based on feed-forward (FFE) alone or in combination with decision-feedback (DFE) schemes.
- A memory-aided technique to enable faster convergence of the adaptive equalizers in the burst-mode upstream approach.
- An AC coupling compensation technique, again for the upstream.

The proposed solutions were first studied at both 25 and 50 Gbps per wavelength and per direction by simulations and then

Manuscript submitted on June 14, 2019.

P. Torres-Ferrera, H. Wang, V. Ferrero and R. Gaudino are with Politecnico di Torino, Department of Electronics and Telecommunications, Torino, Italy. pablo.torres@polito.it.

M. Valvo is with Telecom Italia (TIM), Torino, Italy. maurizio.valvo@telecomitalia.it.

This paper is an extension of the results from previous publications by our group [7-9].

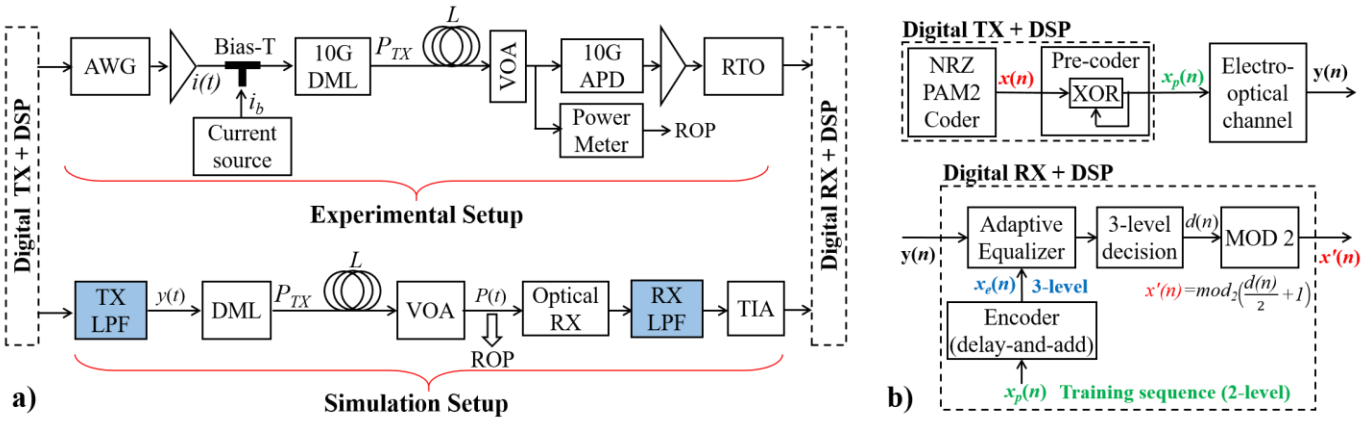

Fig. 1 a) Experimental and simulation setups (local), b) Electrical duobinary (EDB) digital TX and RX block diagrams. The Optical RX block of the simulation setup in a) can be an APD model or a SOA+PIN one (placing an optical filter at SOA output).

they were implemented experimentally in our laboratory. Finally, at 25 Gbps we tested them on an installed metropolitan fiber plant over which we also show the coexistence with previous PON standards, and in particular XGS-PON.

This contribution greatly extends previous works performed by our group in recent years in the field [6-9], in particular including a new set of experiments at both 25 and 50 Gbps data rates, simulations and practical discussions.

The paper is organized as follows: in Section II, the experimental and simulation setups and their details are described, and then in Section III we present our results considering continuous mode transmission for 25 and 50 Gbps PON systems comparing different modulation formats and both equalization schemes. In Section IV, we move to burst-mode upstream DSP proposals for transmission of 25 Gbps electrical duobinary, both in our local premises as well as in the metropolitan field demonstrator. Finally, we wrap-up and discuss our work in Section V.

II. Experimental and Simulation Setup

A. Experimental local setup

Most of our experiments were carried out in a single laboratory location using the setup shown on top of Fig. 1.a, whereas some final experiments shown later used an installed metropolitan fiber testbed. We describe here the details of our experimental setup. An off-line digital transmitter (TX) generates PAM-2, EDB or PAM-4 random sequences that are digital-to-analogue converted by a 92 GSa/s Keysight© arbitrary waveform generator (AWG). Bit rates of 25 Gbps (25G-PON) and 50 Gbps (50G-PON) are used. The modulated electrical signal is amplified to generate the laser current $i(t)$ and, after DC-bias addition, it drives an O-band 1310 nm 10G-class DML. The laser output signal is then launched into 20-km of conventional single-mode fiber (SMF), followed by a variable optical attenuator (VOA) used to set the total optical distribution network (ODN) loss. At the receiver (RX) side, the optical signal is detected by a 10G-class APD, followed by a transimpedance amplifier (TIA), an RF amplifier and a 100 GSa/s Tektronix© real time oscilloscope (RTO) that stores the digital signal. For what concerns the key band-limiting elements (the DML and the APD), we used 10G-class optoelectronics, i.e., hardware solutions similar to the ones used today for XGS-PON, and we extend their use to 25 Gbps and 50 Gbps.

We measured the ODN loss as the difference between the average transmitted power (P_{TX}) at the DML output and the received optical power (ROP) at the APD input. The received digitized signal is off-line processed using an adaptive equalizer (AE) receiver, implemented also in a burst-mode (BM-AE) version [8], described in the following sub-section II.C. We studied three different modulation formats: PAM-2, PAM-4 and EDB. This last one was implemented in a version based on transmission of a binary NRZ pre-coded signal, detected using a duobinary equalizer-based receiver as shown in Fig. 1.b. It was shown in [7] that among all EDB implementations this one gives the best performance in the considered scenario.

B. Simulation setup

To confirm the experimental results and then to extend them to a larger set of parameters, we run numerical simulations according to the schematic shown in the bottom of Fig. 1.a. A standard linear DML model that considers the effect of transient and adiabatic chirp [20-21], with realistic linewidth enhancement factor α = 1.9 and adiabatic chirp coefficient κ = 12 GHz/mW, was used. The SMF chromatic dispersion (CD) effect is also included in the simulator (CD coefficient D = -0.2 ps/nm·km at 1310 nm). In the receiver, noise sources are modelled as additive white Gaussian noise random processes [6]. As optical receiver, we considered two alternatives: the main one is a 10 Gbps APD, and the second one is a SOA+PIN. The APD has responsivity of 0.7 A/W, gain of 8.45 dB, and noise factor of 11 dB. The noise density of the RX is $N_0 = 10^{-21}$ A^2/Hz. These parameters were adjusted from the nominal values indicated in the datasheet of the components to fit the experimental results. Regarding the SOA+PIN approach, the employed model and parameters are described later in sub-section III.C.

In our simulation, we used low-pass filters (LPF) to emulate the frequency response of the TX and RX. Since we want to analyze the performance of the system as a function of the system bandwidth limitation, we used Super-Gaussian filters

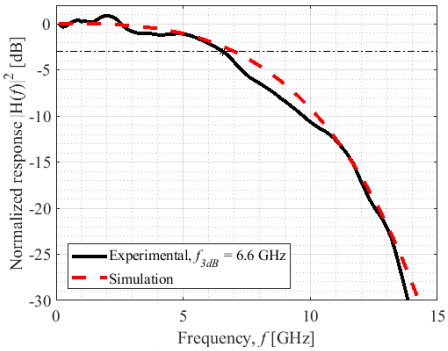

Fig. 2: Frequency response of the full experimental transmission system (solid) and the emulated system frequency response used in our simulations (dashed).

(SGF) which allow changing continuously the -3dB and -20dB frequency (f_{3dB} *and* f_{20dB}) of the filter response, as we already successfully propose in [6]. The frequency response characterization of the full experimental transmission system (including the AWG and RTO) is shown in the solid black curve of Fig. 2, when the DML input bias current is i_b = 60 mA. The most bandlimited device in our experimental setup is the APD+TIA. To match the experimental transfer function in our simulations, we consider a SGF with f_{3dB} = 14 GHz and f_{20dB} = 16 GHz at the TX side [22], and one with f_{3dB} = 7 GHz and f_{20dB} = 13 GHz [23] at the RX side. The resulting total frequency response (TX + RX SGFs concatenation) is shown in the red dashed curve of Fig. 2, which matches very well the experimental data.

C. Burst-mode adaptive equalizer (BM-AE) receiver and fine-time resolved bit error ratio (FTR-BER) metric.

The proposed AE is based on Feed-Forward Equalization (FFE) only or FFE in combination with Decision-Feedback Equalization (DFE), both considering a preamble-aided training stage of length L_{Tr}. The least-mean square (LMS) algorithm is used for coefficient adaptation. For FFE and DFE, 20 and 5 taps are used, respectively. The AE adaptation-rate coefficient (μ) is optimized for every format (μ = $7\text{x}10^{-4}$, $1\text{x}10^{-3}$ and $1\text{x}10^{-3}$ for PAM-2, EDB and PAM-4, respectively; the AE input signal is normalized to have unit power). The equalizer is followed by a decision by amplitude threshold and a decoder block.

For alignment between the RX signal and the BM-AE training sequence, a finite impulse response (FIR)-based block aided by a PRBS header of 2^7 bits inside the TX packets is used. This block acts as a correlator block and automatically finds the beginning of the training preamble inside the RX packets.

After equalization and decoding, the fine-time resolved bit error ratio (FTR-BER) metric is evaluated. As explained in [8], this measurement is better suited than the normal "time-averaged" BER in a burst mode environment, and it is obtained by dividing the data payload in short time slots, then counting the accumulated errors in all the bursts on a time slot basis, as shown in Fig. 3.a. When relevant, the "standard" BER is computed by averaging the FTR-BER over all time slots.

For continuous mode experiments, the length of the training preamble (L_{Tr}) is 2^{14} bits and the length of the payload is 2^{17} bits. For burst-mode experiments, L_{Tr} is a variable parameter

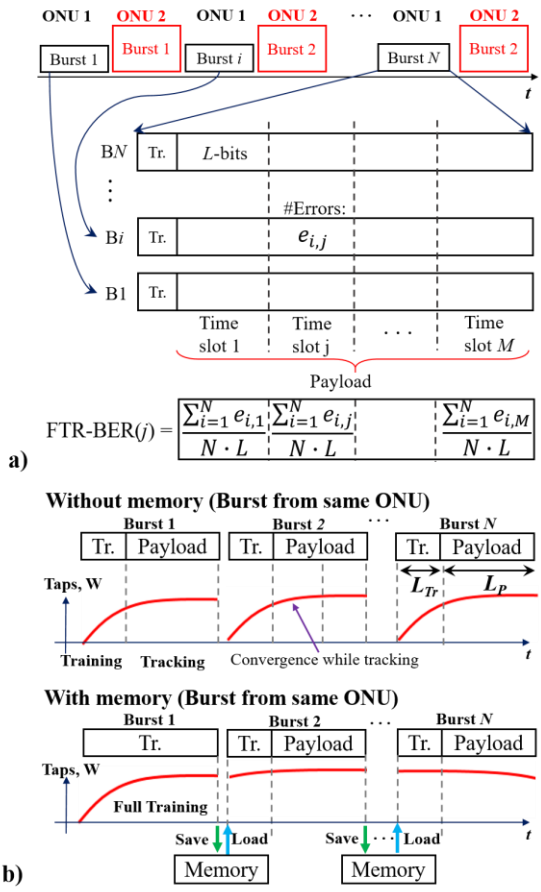

Fig. 3: a) The proposed fine time-resolved BER evaluation scheme, b) burst-mode transmission approaches: memory-less and memory-aided (Tr. stands for training preamble).

and the length of the data payload is the same for all bursts, set equal to 2^{12} minus L_{Tr} bits.

Two BM-AE modes were studied: a normal mode that does not take into account previously received bursts, we call it "memory-less", and a more efficient one, called "memory-aided". In the memory-less approach, the initial tap coefficients of the BM-AE are fixed to zero every time a new burst arrives. On the contrary, in the memory-aided equalizer [8, 24], shown in Fig. 3.b, to initialize the BM-AE at the beginning of each burst we used the same set of tap coefficients that were obtained at the end of the previous burst coming from the same ONU. At the very beginning of the network operation, a single long-burst is sent and equalized in full-training mode to compute the first set of pre-evaluated tap coefficients. In general, every ONU has a different set of optimum tap coefficients. Therefore, the OLT should store one set of taps for every ONU in the network, and be able to re-load from memory the corresponding set every time a burst from a given ONU arrives. This reconfiguration requirement will slightly add complexity and latency to the DSP implementation as compared to a traditional FFE or DFE equalizer, as analyzed in [25,26].

Transmission of N=400 bursts is analyzed. Due to hardware limitations, a simplified scheme in which the amplitude of the received bursts at the input of the BM-AE is assumed to be already equalized (i.e. using a gain control technique [24, 27]), is emulated.

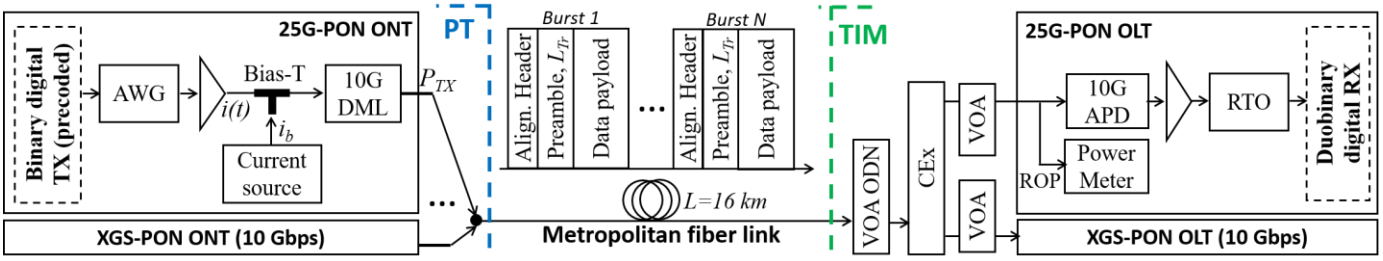

Fig. 4 Metropolitan field demonstrator setup.

D. Metropolitan field demonstrator setup including coexistence with a XGS-PON system.

The metropolitan field experimental setup is shown in Fig. 4. Telecom Italia (TIM) research center in Turin (Italy) and Politecnico di Torino (PT) laboratories are linked using 16 km of installed metropolitan SMF. The used fiber has a significant extra loss because it traverses several central offices and manholes and it is thus a good emulation of a real PON installed link. For the field-trial, we focus on upstream transmission and we placed the Optical Network Termination (ONT) in PT lab and the Optical Line Terminal (OLT) in TIM lab. We test the coexistence of our 25G-PON proposed solution with XGS-PON commercial technology, under burst-mode transmission for both systems. For the XGS-PON, we used commercial devices and a real traffic generator, while for 25G-PON we performed the off-line processing approach described in previous sub-sections. The 25G-PON optical signal is combined with the 10 Gbps XGS-PON 1270 nm upstream signal, and they are then launched into the fiber. At TIM side, a variable optical attenuator (VOA) is used to set the total ODN loss. The 10 and 25 Gbps signals are separated by a coexistence element (CEx) (insertion loss ≤ 1 dB, isolation ≥ 30dB), a device composed of WDM filters to (de)multiplex XGS-PON, G-PON, and NG-PON2 signals, where we have used the GPON port for our 25G-PON wavelength at 1310 nm, and obviously the "regular" port for XGS-PON. The 10 Gbps signal is sent to the XGS-PON OLT and then to a traffic analyzer for bit error count (estimated through a frame loss count). The 25 Gbps is received as explained in previous sub-sections.

When XGS-PON and 25G-PON are transmitting simultaneously on the link to perform coexistence testing, we set the power of the desired (under-test) and interfering signals to obtain a given signal-to-interference ratio (S/I) using two VOAs at OLT side. The minimum S/I that can be set in our experiment was constrained by the sensitivity and maximum transmitted power of each system.

III. Continuous Mode Results

A. Experimental results at 25 and 50 Gbps

After describing our setups, we start by presenting a first set

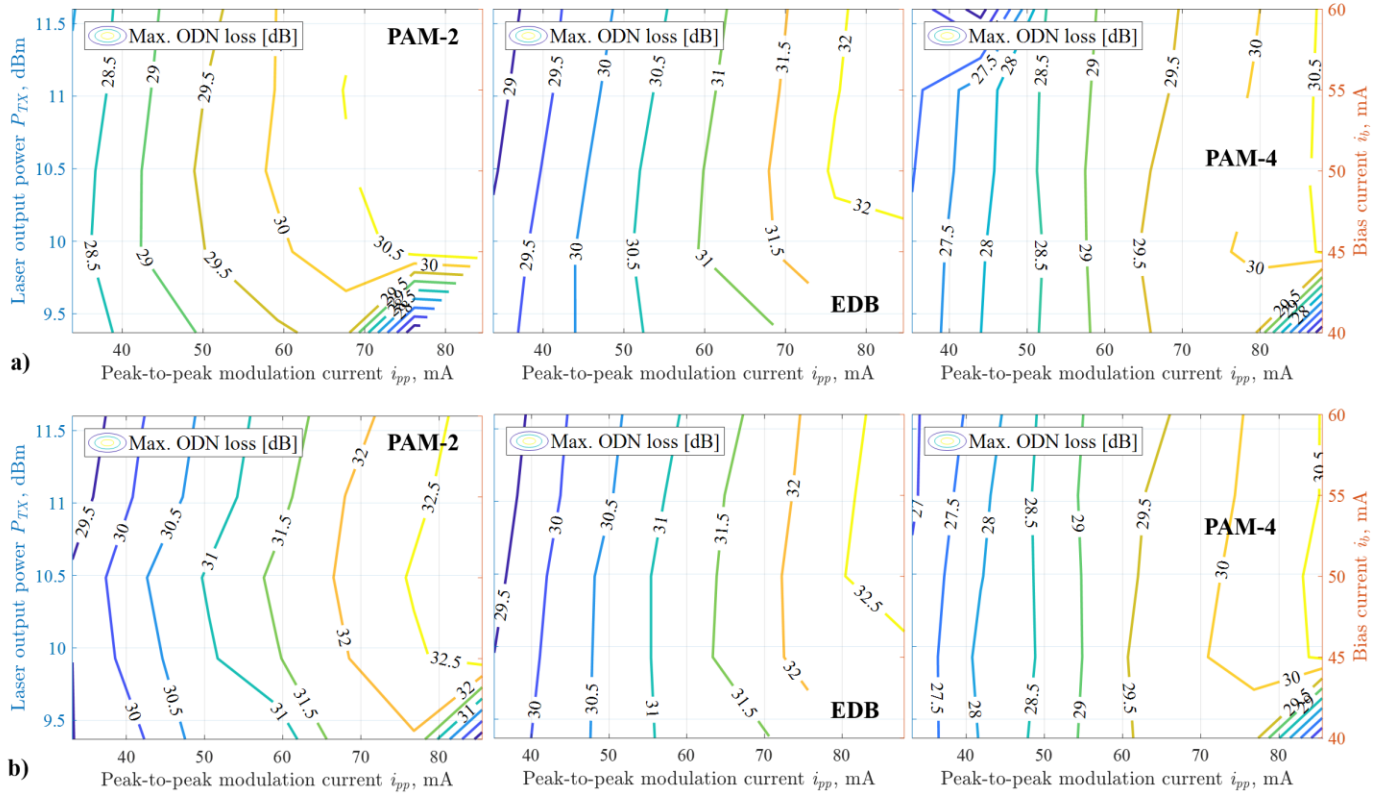

Fig. 5 Maximum ODN loss as a function of TX parameters targeting BER = 10^{-2} for different modulation formats at 25 Gbps data rate, using a) FFE or b) FFE+DFE

of experiments in continuous mode transmission. Our target here is to compare the performance of the modulation formats, the capabilities of the two equalization options (FFE and FFE+DFE) and to optimize the TX parameters. The BER target was set to BER=10^{-2}, as it is currently envisioned in 25G-PON ongoing standardization efforts [2, 3].

In Fig.5, we show for different modulation formats the contour plots of the maximum achievable ODN loss allowing to reach BER=10^{-2} as a function of the bias current of the laser i_b (directly proportional to its output power and bandwidth, and to the extinction ratio (ER)) and of the peak-to-peak amplitude of the modulating signal $i(t)$, i_{pp} (directly related to the ER), for 25 Gbps transmission. Interestingly, an ODN loss ≥29 dB is achievable irrespective of the modulation format and equalization option. When using FFE option (see Fig. 5.a), the best format is EDB, able to reach an ODN loss of up to 32 dB (1.5 dB more than PAM-2 and PAM-4). If DFE is introduced in combination with FFE (see Fig.5.b), the performance of PAM-2 is improved and equals that of EDB. The performance improvement of EDB and PAM-4 is small when DFE is added. Since PAM-2 signal bandwidth is broader than that of EDB and PAM-4 for the same bit rate, the introduction of DFE is more relevant for this format to alleviate bandwidth-limitations penalty that FFE alone is not able to reduce. Since the performance difference between FFE and FFE+DFE is very small for EDB, the addition of DFE is not justified in this case. Moreover, PAM-2 using DFE+FFE is a more complex solution than EDB using FFE only, and both alternatives offer practically the same maximum ODN loss reach. Therefore, results in Fig. 5 indicates that, for 25 Gbps transmission using 10G-class devices, EDB+FFE is in our opinion the best combination of format and equalization option. The suggested maximum current to drive the DML is 100 mA. A combination of i_b = 60 mA and i_{pp} = 80 mA maintains the operation of the DML on the safe side, while guaranteeing an ODN loss of ~32 dB at BER=10^{-2} using EDB+FFE. Therefore, these i_b and i_{pp} values are selected as the DML operating point also for the 25 Gbps burst-mode experiments presented in Section IV. Under this condition, the DML bandwidth is ~14 GHz (the total system bandwidth is ~6.6 GHz, mainly limited by the APD) and its output power is 11.6 dBm.

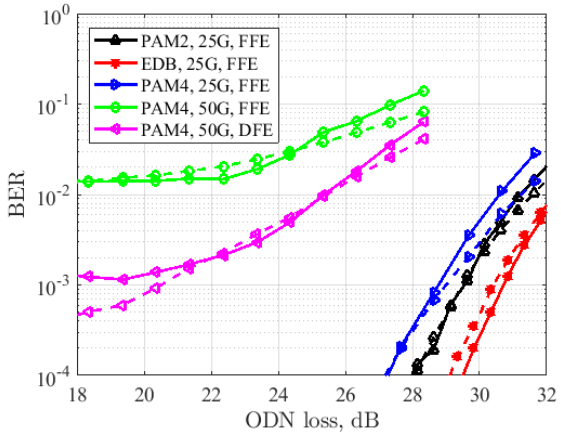

Fig. 6 Comparison of experimental (solid) and simulation (dashed) BER versus ODN loss results for different modulation formats and bit rates. The optimum TX parameters were chosen for each case.

The same optimization procedure was repeated for 50 Gbps transmission using 10G-class devices. In this case, only PAM-4 was experimentally analyzed to keep the maximum baud rate equal to 25 GBaud. The optimum TX parameters either using FFE or DFE+FFE are also i_b = 60 mA and i_{pp} = 80 mA. Fig. 6 shows BER as a function of ODN loss graphs (solid) for 50 Gbps PAM4 under TX optimum conditions comparing FFE and FFE+DFE approaches. For the sake of comparison, 25 Gbps PAM-2, EDB and PAM-4 curves (solid) are also plotted. The big penalty when upgrading from 25 to 50 Gbps is mainly due to extreme electrical bandwidth limitations, while we checked that dispersion penalty is marginal at 1310 nm (since we did not see almost any penalty when comparing back-to-back to 20-km transmission). From Fig. 6, it can be seen that 50 Gbps transmission using 10G-class devices is not possible using PAM-4 + FFE to reach a BER = 10^{-2}, due to the presence of a BER floor. Consequently, the introduction of DFE is mandatory in these conditions. However, even if DFE is used, a maximum ODN loss of only 25 dB is attained, less than the minimum for N1 class PON (29 dB). Anyway, an achievable 25 dB ODN loss can be of interest in some specific future PON scenarios, for instance those meant for ultra-high speed fronthauling, where the requirement on the PON splitting ratio might be possibly relaxed. Otherwise, some alternatives to extend the power budget of 50 Gbps PON systems using bandlimited devices (such as 10G-class ones) have been reported [10-15] recently, using machine-learning equalizer or other advanced DSP techniques, such as Volterra equalizers. However, as discussed in the Introduction, the complexity of these techniques seems to be for the moment really high for medium term implementation.

As an obvious alternative, the use of optoelectronics with higher bandwidth but still using simpler FFE/DFE can be an intermediate feasible solution. This possibility is explored and discussed in next sub-section by using a simulation-based approach for which we first develop a model that matches the experiments presented in this section, and then we use it to study the positive impact of future higher bandwidth optoelectronics. Moreover, in sub-section III.C, we present a preliminary simulation analysis of the feasibility of another optical receiver architecture for 50G-PON which is also under consideration by the research and standardization groups, formed by a SOA, an optical filter and a PIN photodiode.

B. Simulation analysis at 25 and 50 Gbps using APD

In this sub-section we report simulation results obtained using the setup described in sub-section II.B (see bottom of Fig.1.a). BER as a function of ODN loss curves (dashed lines) under different system conditions (in terms of format, equalization and bit rate) are plotted in Fig. 6. A very good agreement between experimental and simulative results was obtained on all curves shown in Fig. 6, thus for different modulation formats and different bit rate, after a simple fitting on the noise level parameters in the simulation.

The target of this sub-section is to understand the required increase in optoelectronic bandwidth to reach at 50 Gbps at least 29 dB ODN loss. We performed simulations changing the APD

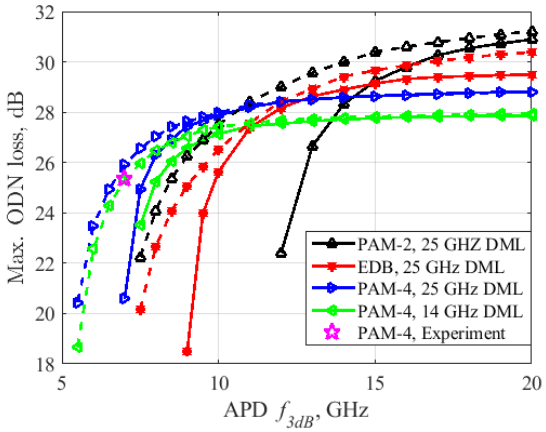

Fig. 7 50 Gbps simulated maximum ODN loss as a function of the APD+TIA f_{3dB}, considering a bandlimited DML with f_{3dB} = 14 GHz for PAM-4 and a broadband DML with f_{3dB} = 25 GHz for PAM-2, EDB and PAM-4. The f_{20dB} of both the DML and APD was selected to keep the same f_{20dB}/f_{3dB} ratio of our experimental devices. Solid graphs for FFE, and dashed graphs for FFE+DFE.

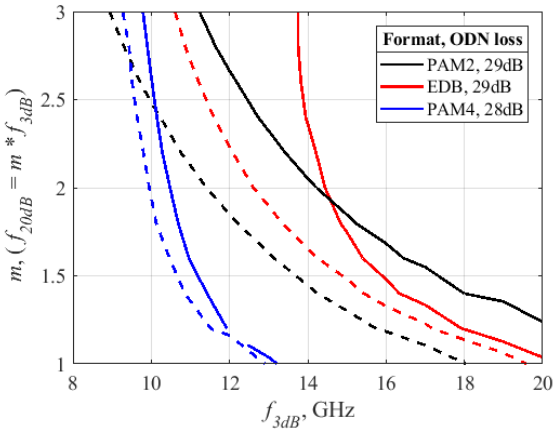

Fig. 8 50 Gbps simulated maximum achievable ODN loss (BER target = 10^{-2}) as a function of the APD f_{3dB} and f_{20dB} parameters ($f_{20dB} = m{\cdot}f_{3dB}$) for different modulation formats. Solid: FFE, dashed: FFE+DFE. The DML f_{3dB} and f_{20dB} are set equal to 25 and 28.6 GHz, respectively.

f_{3dB}, keeping fixed the f_{20dB}/f_{3dB} ratio measured in our experimental device. Two different DMLs were emulated, one with the same f_{3dB} (14 GHz) and f_{20dB} (16 GHz) of our 10G-class experimental device, and the other using higher f_{3dB} and f_{20dB} equal to 25 and 28.6 GHz, respectively. The maximum ODN loss that can be achieved as a function of APD f_{3dB} is shown in Fig. 7 for both DML cases, using FFE or FFE+DFE.

We first analyze PAM-4 format, since it preserves currently available 25 GBaud electronics. By using a bandlimited DML with similar characteristics of our 10G-class experimental device it can be seen that a 29 dB ODN loss cannot be attained even if the APD bandwidth is large. Therefore, broader-band devices should be used at both TX and RX sides. In fact, when DML bandwidth is increased to 25 GHz (a DML with this characteristics is reported in [4]), an ODN loss of 28.5 dB can be achieved with an APD $f_{3dB} \geq$ 15 GHz. The advantage of including DFE is evident for low f_{3dB} values, whereas for f_{3dB} higher than 10 GHz, both FFE and FFE+DFE approaches exhibit similar performance. However, even if using broader-band devices and DFE, the minimum 29 dB ODN loss cannot be achieved with PAM-4 at 50 Gbps. One solution to achieve the required power budget is to increase slightly the TX power of the laser (currently 11.5 dBm). Another alternative is employing other modulation formats, such as PAM-2 or EDB, with 50 GBaud baud rate. Assuming electrical interfaces able to work at this baud rate, in Fig. 7 we plot the EDB and PAM-2 curves assuming the same conditions as for 50 Gbps PAM-4 simulations. The 29 dB power budget can be achieved with both PAM-2 and EDB using the proper value of APD f_{3dB} in combination with FFE or FFE+DFE equalizer. Therefore, the modulation format choice depends on a trade-off between bandwidth of the devices and TX/RX complexity.

The results shown in Fig. 7 were obtained using a fixed f_{20dB} value for every f_{3dB}. However, APD devices with same f_{3dB} can have different steepness (i.e. f_{20dB}) [6]. To analyze the effect of this latter parameter in the performance of the 50 Gbps systems, contour plots of maximum ODN loss as a function of the APD f_{3dB} and f_{20dB} are plotted in Fig. 8. A DML with f_{3dB} = 25 GHz and f_{20dB} = 28.6 GHz is considered. Fig. 8 indicates the required APD f_{3dB} and f_{20dB} pairs to achieve a maximum ODN loss of at least 29 dB (28 dB in the case of PAM-4), which are those above and to the right of a given contour curve (one curve for every format, solid for FFE and dashed for DFE). From Fig. 8 we can extract the following conclusions. We confirm, also for the 50 Gbps analyzed scenario, that DFE provides an effective power gain for PAM-2, irrespective of the steepness of the APD frequency response. For EDB, the gain provided by DFE increases when steepness decreases, being small for high steepness values ($f_{20dB} < 1.5 f_{3dB}$). PAM-4 is less sensitive than PAM-2 and EDB to variations of the steepness of the filters since the contour curves are more vertical, especially when $f_{20dB} \geq 1.5 f_{3dB}$. Apart from this, PAM-2 is the best format if DFE is added to the RX scheme, and the TX has enough bandwidth. If we want to avoid using DFE to reduce complexity, EDB outperforms PAM-2, in the analyzed 50 Gbps scenario, only in some conditions (i.e. high steepness: $f_{20dB} < 1.5 f_{3dB}$).

C. Simulation analysis at 50 Gbps replacing APD by SOA+PIN

Although our contribution is focused on an APD-based PON setup, there is another architecture that is also being investigated by the research and standardization groups to develop the 50G-PON transceivers. This alternative architecture uses a combination of a SOA and a PIN photodiode as optical receiver. An optical filter is placed in between SOA and PIN to filter out part of the optical noise generated by the SOA. In this sub-section, we perform a preliminary analysis to explore by means of simulation this alternative. The SOA+PIN receiver has two features that can be useful in the 50G-PON bandlimited scenario. The first one is that the 10G-class PIN photodiodes can have higher f_{3dB} than APDs. The second one is that SOAs can provide higher gain than APDs. We use here the same simulation setup and parameters reported in previous sub-section III.B, but just replacing the APD model by the SOA+PIN one, placing an optical filter at the output of the amplifier. We used a simplified model for the SOA, assuming a linear regime with gain of 12 dB, and a noise figure of 9 dB. For the PIN, a responsivity of 0.7 A/W was set and the effect of

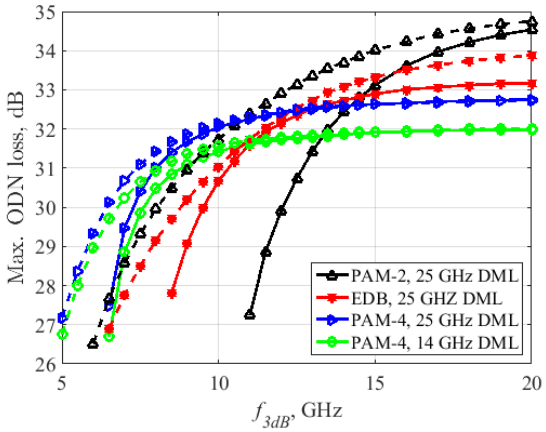

Fig. 9 SOA+PIN alternative receiver: 50 Gbps simulated maximum ODN loss as a function of the receiver f_{3dB}, considering a bandlimited DML with f_{3dB} = 14 GHz for PAM-4 and a broadband DML with f_{3dB} = 25 GHz for PAM-2, EDB and PAM-4. The f_{20dB} of both the DML and the receiver was selected to keep a fixed f_{20dB}/f_{3dB} ratio. Solid graphs for FFE, and dashed graphs for FFE+DFE.

shot noise was taken into account. The amount of thermal noise, mainly added by the TIA, is set the same as in the APD based receiver ($N_0 = 10^{-21}$ A^2/Hz). The optical passband filter placed between the SOA and the PIN is modeled as a fifth order super-Gaussian filter with -3dB bandwidth of 400 GHz. We consider accurate enough the assumption of SOA linearity, since the SOA is used here as a receiver pre-amplifiers, and thus the average input power in the analyzed scenario is fairly low, ranging from -27 to -15 dBm.

By using the described model and parameters, we reproduced similar graphs as those shown in Fig. 7, but now using the SOA+PIN optical receiver. The obtained results are plotted in Fig. 9, from which it can be seen that the target ODN loss can be achieved even with bandlimited 10G-class optoelectronic devices. For example, a 14-GHz DML in combination with a 7-GHz SOA+PIN guarantee 29 dB of power budget if PAM-4 and FFE are used and a less bandwidth constrained SOA+PIN would allow power budgets in excess of 32 dB with PAM-2. Therefore, the SOA+PIN alternative seems to be a good candidate to implement 50G-PON. However, these results are just preliminary, and more detailed parametric analyses and experimental verification, out of the scope of the present contribution focused on APD receiver, need to be performed

IV. 25 Gbps EDB Burst Mode Experimental Results

In this Section, we report the experimental results obtained in burst-mode transmission using EDB format in combination with BM-AE based on FFE, targeting 25 Gbps transmission. We selected EDB format and FFE equalization since this combination resulted to be the more convenient for 25 Gbps according to the analysis performed in previous section. In following sub-sections, we show the advantages of using memory-aided BM-AE and the need to characterize the performance of BM-AE using the FTR-BER metric. Then, we compare the performance of the 25G-PON system in burst-mode against continuous mode, both with and without interfering XGS-PON transmission using a metropolitan field demonstrator. Finally, we discuss about the AC coupling effect in our analyzed burst-mode system and a technique to reduce it.

A. Burst-mode transmission using the memory-aided approach

After setting the optimum TX parameters obtained for continuous mode, several bursts were transmitted, stored and off-line post-processed as explained in Section II.C, using the metropolitan experimental setup shown in Fig. 4. An appropriate burst on and off duration of 0.5 and 0.1 μs, respectively, was selected in order to minimize the AC-coupling effect (see sub-section IV.C). After equalization and decoding, the payload of the bursts was divided in time-slots to compute the FTR-BER (see Section II.C). The purpose of evaluating the FTR-BER metric (somehow an "instantaneous" BER [8]) is to select the minimum length of the BM-AE training preamble (thus increasing the system transmission efficiency) that guarantees a BER below the target since the very beginning of the payload. We observed that under some conditions (for instance, a short-training stage), the BM-AE keeps adapting after the training stage (i.e. during the tracking stage) before reaching convergence (see Fig. 10.a). Therefore, if training is not long enough, the initial bits of the payload are more likely to be wrong than the rest, which results on a non-uniform distribution of the errors along the payload. By just taking into account the standard BER metric (evaluated as the total number of errors divided by the total number of bits in the

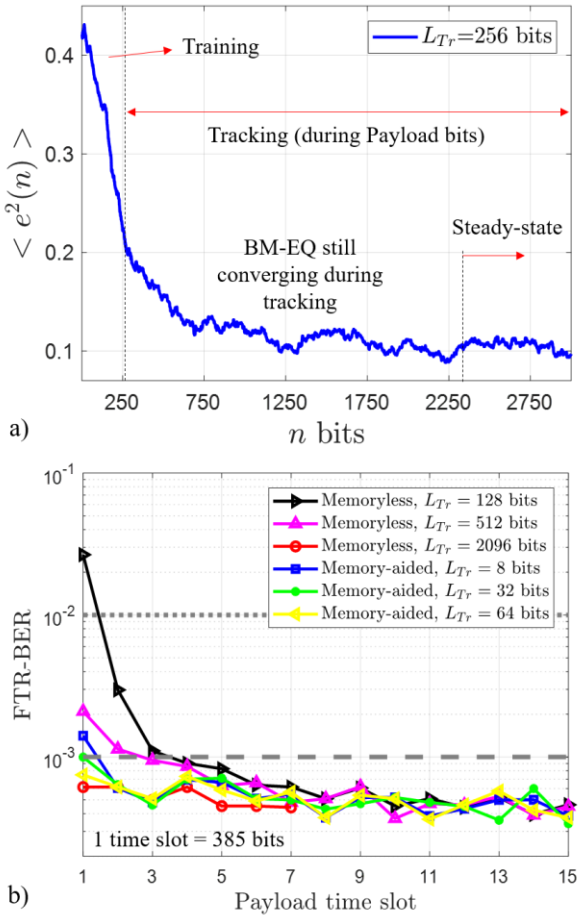

Fig. 10 a) Error square evolution over time for a given L_{Tr}; b) FTR-BER over each of the 385-bits time slots for memory-aided and memoryless BM-AE approaches with different training length L_{Tr}. ODN loss = 28.7 dB.

full payload), the fact that there is a higher concentration of errors at the beginning of the payload, that would lead to a FEC-failure condition, can remain completely hidden. In this context (and similar situations as that described in sub-section IV.C related to the AC-coupling effect), having an "instantaneous" BER metric (i.e. FTR-BER) becomes helpful.

Following the previous ideas, we analyze the performance of the 25G-PON system in burst-mode by using the FTR-BER metric and setting an ODN loss close to 29 dB [9]. BM-AE memory-aided and memoryless approaches are compared in terms of FTR-BER as a function of payload time-slots for different lengths of the training stage. The obtained results are plotted in Fig. 10.b. While the memoryless BM-AE needs ~2000 bits to converge, thus guaranteeing a uniform error distribution along the full payload (see curve with circles, in which FTR-BER is flat), the memory-aided approach requires a much shorter training stage (64 bits) to attain the same condition, showing the advantages of using this second approach. For L_{Tr} values less than ~2000 bits, for instance 128 and 512 bits, there is a non-uniform performance along the payload for the memoryless case, as shown in Fig. 10.b. Therefore, even if the average BER over the full payload can fulfill the BER target (i.e. 10^{-2} or 10^{-3}), the first slots will produce a FEC-failure. In the memory-aided case, the same problem occurs if $L_{Tr} \leq 64$ bits. Therefore, a short-training stage is still needed (although memory-aided approach is used) to remove a short amount of errors at the beginning of the payload due to the remaining AC-coupling effect (minimized, but not absent) and not because of needing transient removal due to equalizer adaptation. Once a uniform error distribution along the payload is verified (thus avoiding the risk of masking failure BER conditions), the standard BER is evaluated for every ODN loss value by counting the errors in the full payload of all bursts. The BER thus obtained is graphed as a function of ODN loss for memory-aided burst-mode transmission (L_{Tr} = 64 bits) in Fig. 11.a (curve with circles) [9]. For the sake of comparison, the 25 Gbps EDB continuous mode BER versus ODN loss curve obtained under the same experimental conditions is also plotted in Fig. 11.a (curve with squares). The burst-mode operation introduces a penalty of 1 dB at BER = 10^{-2}. In [28-29], a 10 Gbps special multi-electrode distributed feedback laser that achieves a reduced burst-mode penalty is proposed. Since an ODN loss higher than 29 dB (BER=10^{-2}) can be achieved in our burst-mode transmission, in this work we just tolerated the introduced penalty.

B. Metropolitan field demonstration results for upstream transmission

The coexistence of 25G-PON and XGS-PON technologies is analyzed in this sub-section, using the metropolitan field demonstrator described in sub-section II.D. To this purpose, we performed the 25G-PON BER versus ODN loss measurements [9], for burst and continuous modes, under the same assumptions reported in previous sub-section but now turning on the XGS-PON transmission (interference signal) setting it a stronger ROP than that of 25G-PON (to have a fixed S/I = -17 dB irrespective of the ODN loss). The obtained curves are

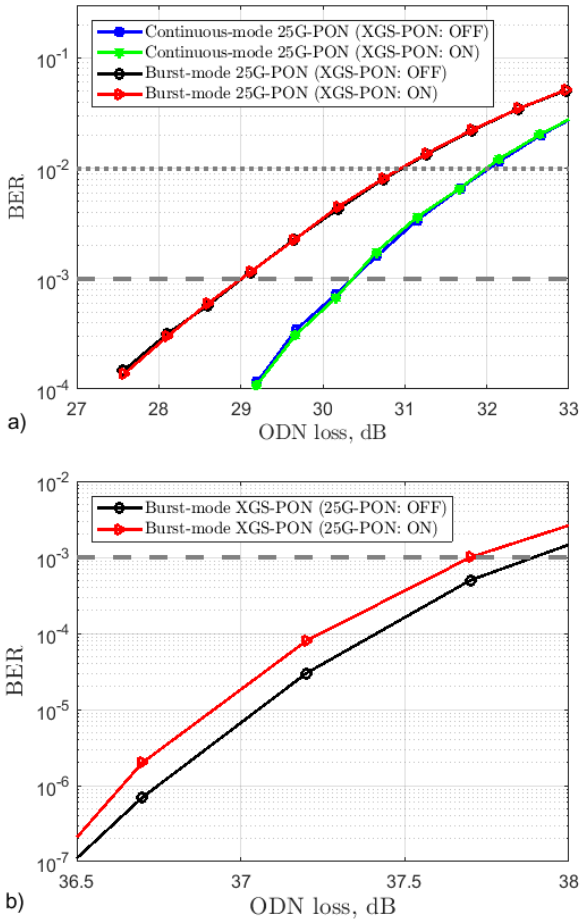

Fig. 11 System performance as a function of ODN loss under different scenarios [9]; a) 25G-PON under test and XGS-PON interfering with a S/I = -17 dB; b) XGS-PON under test and 25G-PON interfering with a S/I = -20 dB.

shown in Fig. 11.a (curves with stars and triangles). A negligible penalty due to XGS-PON interference can be observed (less than 0.1 dB in both burst and continuous modes). A 31 dB (BER=10^{-2}) ODN loss can be attained, in 25G-PON burst-mode transmission in coexistence with legacy technology.

The influence of the 25G-PON signal on the XGS-PON one is also tested. The performance of the XGS-PON system (burst-mode) was measured in two conditions: 25G-PON turned off and on (setting an S/I = -20 dB in the latter case). The obtained post-FEC BER values as a function of the ODN loss are plotted in Fig.11.b. A marginal penalty due to 25G-PON interference is also observed in this case (less than 0.2 dB difference between both curves for any BER value). Therefore, a feasible full coexistence operation between 25G-PON and XGS-PON is demonstrated.

C. AC coupling effect compensation

In our experimental setup, some devices are AC-coupled, which produces baseline-wandering effect [30-32]. This phenomenon results in a performance penalty if it is not somehow reduced. In previous sub-sections IV.A and IV.B the AC-coupling effect was highly reduced by just setting an adequate on and off burst durations. Since we wanted to analyze the effect of other impairments, this simple method was useful

to avoid the baseline-wandering penalty. However, in a practical situation, the adopted method cannot be used, since the off duration is in general much longer, depending on the amount of total upstream traffic generated from different ONUs. Therefore, in this sub-section we present a DSP-aided method to compensate for the AC-coupling effect at the receiver side. The on and off burst duration (ΔB) is now set practically identical (just 50 ns longer in off state) in order to enhanced the AC coupling effect and be able to measure the effectiveness of our adopted solution.

Whereas several of our laboratory devices are AC-coupled, in commercial implementations all the devices are intended to be DC-coupled to avoid the baseline wandering effect, especially at the transmitter side. However, even some devices used in commercial applications can still be AC-coupled, such as the APD, particularly in high-bandwidth versions. Therefore, the analysis performed in this sub-section is not only useful for lab experimental purposes, but also for commercial implementations.

The AC-coupling effect can be modelled in a simplified way as a first-order high-pass filter (HPF). A first-order digital HPF with gain of unity in the pass-band is given by Eq. (1) in the *Z*-transform domain. The relation between the HPF cut-off frequency f_c and β is given by Eq. (2).

$$H_{AC}(z) = \left(\frac{\beta+1}{2}\right)\frac{z-1}{z-\beta} \tag{1}$$

$$\beta = \frac{1-\sin(2\pi f_c)}{\cos(2\pi f_c)} \tag{2}$$

A modified inverse HPF to reverse the effect of AC-coupling, modelled as Eq.(1), in the received signal, is obtained by inverting the response of $H_{AC}(z)$ and shifting the pole slightly to the origin to avoid DC infinite amplification and instability [33]. The resulting inverse HPF, called here AC-coupling equalizer (ACEQ), $H_{ACEQ}(z)$, is given by Eq. (3). The parameter γ is related to the maximal gain A (at DC) as shown in Eq. (4).

$$H_{ACEQ}(z) = \left(\frac{\gamma+1}{\beta+1}\right)\frac{z-\beta}{z-\gamma} = \left(\frac{\gamma+1}{\beta+1}\right)\frac{1-\beta z^{-1}}{1-\gamma z^{-1}} \tag{3}$$

$$\gamma = 1 - 2\frac{1-\beta}{\mathrm{A}(\beta+1)+1-\beta} \tag{4}$$

By using the setup shown in Fig. 1, we experimentally tested the effectiveness of the AC-coupling equalizer. We optimized β and γ parameters to minimize BER in a worst-situation case, and then we kept them fixed. The ACEQ is applied to the received signal $y(n)$ before entering the BM-AE. After AC-coupling compensation, the signal is processed as explained in previous sub-sections. The obtained results are shown in Fig. 12. BER as a function of received optical power (ROP) curves are shown in Fig. 12.a, setting two different burst durations (ΔB = 0.5 μs and 1.0 μs) and comparing the performance with (dashed curves) or without (solid curves) the ACEQ. A power gain is observed for both burst-duration cases, being more evident for the ΔB = 1.0 μs one. In this case, a power gain of 1 dB at BER=10^{-2} is achieved by using the ACEQ. The effect of the ACEQ can be qualitatively observed in the inset of Fig. 12.a that shows the received signal before and after the ACEQ for a ROP = -14.8 dBm (low RX noise situation). Regarding the ΔB = 0.5 μs case, a sensitivity of -19.7 dBm can be achieved by compensating the AC-coupling effect, which results in an achievable ODN loss of 31.3 dB (P_{TX} = 11.6 dBm). This value matches well the maximum ODN loss achieved using reduced AC-coupling conditions presented in Section IV.A (see the circled curved of Fig. 11.a).

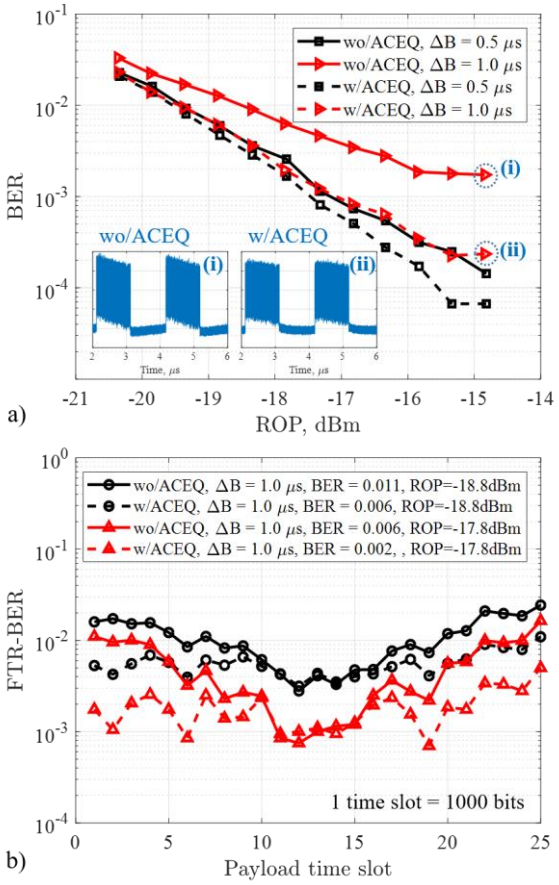

Fig. 12 a) BER as function of received power, comparing the performance with and without ACEQ for different burst duration, b) FTR-BER as a function of time for two specific ROP values comparing the performance with and without ACEQ. Memory-aided BM-AE with L_{Tr} = 64 bits is used.

The BER results presented in Fig. 12.a. were obtained by averaging the errors over the full-payload. To further analyze the effectiveness of the ACEQ, we select two cases corresponding to two ROP values equal to -17.8 dBm and -18.8 dBm (BER around 10^{-2}), and plot the FTR-BER (see section II.C) using and not using the ACEQ technique. The corresponding results are shown in Fig. 12.b. The AC-coupling impact when not compensated (solid graphs) can be clearly observed: at both the beginning and end of the burst the FTR-BER is notoriously higher than at the center. This FTR-BER distribution is obtained because the decision thresholds of the BM-AE become optimized at the middle of the burst. When ACEQ is applied, the FTR-BER is flattened (especially if the SNR is higher, i.e. higher ROP values), which is a desired effect to avoid FEC-failure conditions caused by accumulation of

errors in just some particular slots of the burst payload. Therefore, the effectiveness of the used ACEQ technique is further verified.

V. Conclusion

We have studied in this paper several solutions to enable 25G-PON and 50G-PON by using simple but effective DSP at the receiver side, and we tested them experimentally. We showed in our lab and field-trial setups that 25G-PON is feasible in O-band targeting 29 dB ODN loss even when using legacy 10G-class optoelectronics, including DML lasers. The situation is significantly more critical for 50G-PON, which for sure will require higher bandwidth components to achieve high ODN loss, as we studied by simulations. We showed that using optoelectronic devices for 25G-class binary transmission, the target 29 dB could be attained, anyway without significant margin. To achieve even higher ODN losses (or at least 29 dB with a reasonable margin), it seems that optically amplified solutions need to be introduced.

We have not considered here an even further evolution toward 100 Gbps per wavelength. It is anyway evident from our results at 50 Gbps, that due to the specific characteristics of PON (in particular the very high target ODN loss, which is enormously higher than, for instance, the one for intra-data center applications at the same speed), the next step towards 100G-PON (per wavelength) would be very critical if sticking with single-wavelength direct-detection approaches. In fact, even if the optoelectronics have a sufficient bandwidth, the resulting power budget may not be enough. Besides the obvious option of using 2-4 wavelengths in parallel to reach 100 Gbps, completely new roads should be investigated, including coherent detection solutions applied to PON.

Acknowledgment

This work was carried out under the PhotoNext initiative at Politecnico di Torino (http://www.photonext.polito.it/) and inside a research contract with Telecom Italia (TIM).

References

[1] E. Harstead, D. van Veen, V. Houtsma, P. Dom, "Technology Roadmap for Time-Division Multiplexed Passive Optical Networks (TDM PONs)," *Journal of Lightwave Technology*, vol. 37, no. 2, pp. 657-664, 2019.

[2] "IEEE P802.3ca 50G-EPON Task Force", [Online] Available: http://www.ieee802.org/3/ca/, accessed 13 June 2019.

[3] ITU-T, "G.Sup64 PON transmission technologies above 10 Gbit/s per wavelength", 2018.

[4] S. H. Bae, Hoon Kim, and Y. C. Chung, "Transmission of 51.56-Gb/s OOK signal using 1.55-μm directly modulated laser and duobinary electrical equalizer," *Opt. Express*, vol. 24, pp. 22555-22562, 2016.

[5] V. Houtsma and D. van Veen, "A Study of Options for High-Speed TDM-PON Beyond 10G," *Journal of Lightwave Technology*, vol. 35, no. 4, pp. 1059-1066, 2017.

[6] P. Torres-Ferrera, V. Ferrero, M. Valvo, R. Gaudino, "Impact of the Overall Electrical Filter Shaping in Next-Generation 25 and 50 Gb/s PONs", *Journal of Optical Communications and Networking*, vol. 10, no. 5, pp. 493-505, 2018.

[7] P. Torres-Ferrera, V. Ferrero, R. Mercinelli, R. Gaudino, "Experimental Demonstration of DSP-Assisted Electrical Duobinary Optimization for High Speed PON 25+ Gbps Using 10 Gbps APD Receiver", *Proc. European Conference Optical Communications (ECOC)*, 2018, Paper Mo4B.2.

[8] P. Torres-Ferrera, V. Milite, V. Ferrero, M. Valvo, R. Mercinelli, R. Gaudino, "Burst-mode Equalisation Strategies in 25 Gbps US-PON using Duobinary and 10G-class APD for 20-km in C-band", *Proc. Optical Fiber Communication Conference (OFC)*, 2019, paper W4J.1.

[9] P. Torres-Ferrera, H. Wang, V. Ferrero, A. Pagano, M. Valvo, R. Mercinelli, R. Gaudino, "Field Demonstration of 25G-PON and XGS-PON Burst-Mode Upstream Coexistence", *Proc. European Conference Optical Communications (ECOC)*, 2019 [Accepted].

[10] K. Zhang, Q. Zhuge, H. Xin, W. Hu, D. V. Plant, "Performance comparison of DML, EML and MZM in dispersion-unmanaged short reach transmissions with digital signal processing," *Opt. Express*, vol. 26, pp. 34288-34304, 2018.

[11] M. Tao, L. Zhou, H. Zeng, S. Li, and X. Liu, "50-Gb/s/λ TDM-PON Based on 10G DML and 10G APD Supporting PR10 Link Loss Budget after 20-km Downstream Transmission in the O-band," *Proc. Optical Fiber Communication Conference*, 2017, paper Tu3G.2.

[12] X. Tang, Y. Qiao, J. Zhou, M. Guo, J. Qi, S. Liu, X. Xu, and Y. Lu, "Equalization scheme of C-band PAM4 signal for optical amplified 50-Gb/s PON," *Opt. Express*, vol. 26, pp. 33418-33427, 2018.

[13] V. Houtsma, D. van Veen, "Bi-Directional 25G/50G TDM-PON With Extended Power Budget Using 25G APD and Coherent Detection," *Journal Lightwave Technol.*, vol. 36, pp.122-127, 2018.

[14] P. Li, L. Yi, L. Xue, and W. Hu, "56 Gbps IM/DD PON based on 10G-Class Optical Devices with 29 dB Loss Budget Enabled by Machine Learning," *Proc. Optical Fiber Communication Conference*, 2018, paper M2B.2.

[15] V. Houtsma, E. Chou, and D. van Veen, "92 and 50 Gbps TDM-PON using Neural Network Enabled Receiver Equalization Specialized for PON," *Proc. Optical Fiber Communication Conference (OFC)*, 2019, paper M2B.6.

[16] L. Yi, T. Liao, L. Huang, L. Xue, P. Li, W. Hu, "Machine Learning for 100 Gb/s/λ Passive Optical Network," *J. Lightwave Technol*. vol. 37, pp. 1621-1630, 2019.

[17] P. Li, L. Yi, L. Xue, and W. Hu, "100Gbps IM/DD Transmission over 25km SSMF using 20G-class DML and PIN Enabled by Machine Learning," *Proc. Optical Fiber Communication Conference*, 2018, paper W2A.46.

[18] J. Zhang, J. S. Wey, X. Huang, "Experimental Results of Single Wavelength 50 GPON", IEEE 802.3c Meeting, Nov. 2017, zhang_junwen_3ca_1_1117.

[19] V. Houtsma, D. van Veen, R. Bonk, "Options for Single wavelength 50G TDM-PON", IEEE 802.3c Meeting, Sep. 2017, houtsma_3ca_1_0917.

[20] D. A. Ackerman *et al*., "Telecommunication Lasers," in Optical Fiber Telecommunications, volume IVA, Elsevier, pp. 613-625, 2002.

[21] C. R. Campos, A. Consoli, J. M. R. Campos, P. R. Horche, "Impact on the chirp effect of the shaped electrical-driven current of the directly-modulated VCSEL in an optical fiber link," *Optics Communications* 435, pp. 326-333, 2019.

[22] Gooch and Housego, High Bandwidth DFB lasers 1310 nm AA0701 model, [Online] Available: https://goochandhousego.com/product-categories/dfb-lasers-modules/, accessed 13 June 2019.

[23] Discovery Semiconductors Inc, 10 Gb/s APD+TIA Optical Receiver with optional CDR, DSC-R402APD model, [Online] Available: https://www.discoverysemi.com/Product_Pages/DSCR402APD.php, accessed 13 June 2019.

[24] R. Koma, *et al*., "Burst-Mode Digital Signal Processing That Pre-Calculates FIR Filter Coefficients for Digital Coherent PON Upstream", *Journal of Optical Communications and Networking*, vol. 10, no. 5, pp. 461-470, 2018.

[25] P. K. Meher, "New Approach to Look-Up-Table Design and Memory-Based Realization of FIR Digital Filter," in IEEE Transactions on Circuits and Systems I: Regular Papers, vol. 57, no. 3, pp. 592-603, 2010.

[26] M. Kumm, K. Möller and P. Zipf, "Dynamically reconfigurable FIR filter architectures with fast reconfiguration," 2013 8th International Workshop on Reconfigurable and Communication-Centric Systems-on-Chip (ReCoSoC), Darmstadt, pp. 1-8, 2013.

[27] M. D. Santa, C. Antony, G. Talli, P. Townsend, "Variable Gain SOA Pre-Amplifier for Optical Equalization of a 25Gb/s Burst-Mode PON Upstream with 10G Optics," *Proc. Optical Fiber Communication Conference (OFC)*, 2019, W4J.2.

[28] S. Porto, D. van Veen, V. Houtsma, N. Basavanhally, C. Bolle, H. Schmuck, P. D. Townsend, M. Earnshaw, and T. Pfeiffer, "10Gb/s Low-Cost Directly Modulated Multi-Electrode Laser with Suppressed Thermal Wavelength Drift for Burst-Mode Upstream Transmission in TWDM-PONs," *Proc. Optical Fiber Communication Conference*, 2018, paper Th1E.3.

[29] D. van Veen, V. Houtsma, S. Porto, N. Basavanhally, C. Bolle and H. Schmuck, "Wavelength-stable burst-mode laser for next-generation PONs," in *Journal of Optical Communications and Networking*, vol. 11, no. 2, pp. A155-A165, 2019.

[30] H. Nakamura *et al*., "AC-Coupled Burst-Mode Transmitter Using Baseline-Wander Common-Mode-Rejection Technique for 10-Gbit/s-Class

PON Systems," in *Journal of Lightwave Technology*, vol. 27, no. 3, pp. 336-342, 2009.
[31] J. Zhuang, B. Doyle and E. Fang, "Linear Equalization and PVT-Independent DC Wander Compensation for AC-Coupled PCIe 3.0 Receiver Front End," *IEEE Transactions on Circuits and Systems II: Express Briefs*, vol. 58, no. 5, pp. 289-293, 2011.
[32] E. Rotem and D. Sadot, "Performance analysis of AC-coupled burst-mode receiver for fiber-optic burst switching networks," *IEEE Transactions on Communications*, vol. 53, no. 5, pp. 899-904, 2005.
[33] R. Abächerli, J. Isaksen, R. Schmid, R. Leber, H-J. Schmid, G. Generali "Digital DC-Reconstruction of AC-Coupled Electrophysiological Signals with a Single Inverting Filter", *Plus One*, vol. 11, no. 3: e0150207, 2016.

Pablo Torres-Ferrera received the B.Eng., M.E.E. and Ph.D. degrees (with honors) in telecommunications in 2010, 2012 and 2017, respectively, from the National Autonomous University of Mexico (UNAM), Mexico City. He worked from 2012 to 2013 at Huawei Technologies Mexico in the implementation of OTN rings. As part of his PhD investigation work, he carried out research internships at Athens Information Technology (AIT), Greece, in 2014 and at Politecnico di Torino, Italy, in 2016. Since 2017, he is a Post-Doctoral Researcher at Politecnico di Torino, working in the field of high-speed optical access networks and data-center interconnects.

Haoyi Wang received the bachelor degree in Telecommunication Engineering in 2015, and the master degree in Communication and Computer Networks Engineering in 2018, both from Politecnico di Torino, Italy. Now, she is a Ph.D. candidate in Electrical, Electronics and Communication Engineering at Politecnico di Torino. Her current research interest includes the area of high-speed optical access networks.

Valter Ferrero (M'97) received the Laurea degree (summa cum laude) in Electronics Engineering in 1994 from Politecnico di Torino, Italy. In 1994, he collaborated with Politecnico di Torino, working on coherent optical systems. From 1995 to 1996, he was with GEC Marconi (now Ericson), Genova, Italy. In 1997, he was in charge of the Optical Laboratory, Department of Electrical Engineering, Politecnico di Torino, became Assistant Professor in 2001 and Associate Professor in 2018. He is author or co-author of more than 80 papers in the field of Optical Communications. He is currently with the Optical Communications Group, Politecnico di Torino. His current research interests include optical coherent communications, free-space optical communications, and next-generation passive optical networks.

Maurizio Valvo received his MSc degree in electronics engineering cum laude at the University of Naples (Italy) in 1991. In the same year, he joined CSELT, the center for research in Telecommunications, now TIM Lab - Turin where he is currently active. He has focused since the beginning of his career on broadband access networks and in particular on PON systems, which he has also contributed to specify, develop and test during the 90's in the framework of several European funded projects. He has led research projects with the objective to specify and test, both in the laboratory and in the field, innovative access network technologies based on PON, xDSL, HFC, Wimax and free space optics. Currently he leads the laboratory for fixed access network innovation and a research project for the innovation of the Telecom Italia optical access network. He holds four patents and is co-author of three books and several papers.

Roberto Gaudino Ph.D., is currently Full Professor at Politecnico di Torino, Italy. His main research interests are in the long haul DWDM systems, fiber non-linearity, modelling of optical communication systems and in the experimental implementation of optical networks, with specific focus on access networks. In particular, in the last five years, he focused his activity on short-reach optical links using plastic optical fibers (POF) and on next-generation passive optical access networks (NG-PON2). Currently, he is working on ultra-high capacity systems for medium reach links. Previously, he worked extensively on fiber modelling, optical modulation formats, coherent optical detection, and on the experimental demonstration of packet switched optical networks. He is author or co-author of more than 200 papers in the field of Optical Communications. From 2009 to 2016 he was the coordinator of three projects in the area of optical access (EU FP6-IST STREP "POF-ALL" and "POF-PLUS" and EU FP7-ICT STREP project "FABULOUS"). He is now the coordinator of the PhotoNext center at POLITO.